Open Access

Maziar Sedighi Moghaddam*, Jan Van den Bulcke, Magnus E.P. Wålinder, Per M. Claesson, Joris Van Acker and Agne Swerin

Microstructure of chemically modified wood using X-ray computed tomography in relation to wetting properties

DOI 10.1515/hf-2015-0227
Received October 21, 2015; accepted August 24, 2016; previously published online October 8, 2016

Abstract: X-ray computed tomography (XCT) was utilized to visualize and quantify the 2D and 3D microstructure of acetylated southern yellow pine (pine) and maple, as well as furfurylated pine samples. The total porosity and the porosity of different cell types, as well as cell wall thickness and maximum opening of tracheid lumens were evaluated. The wetting properties (swelling and capillary uptake) were related to these microstructural characteristics. The data show significant changes in the wood structure for furfurylated pine sapwood samples, including a change in tracheid shape and filling of tracheids by furan polymer. In contrast, no such changes were noted for the acetylated pine samples at the high resolution of 0.8 μm. The XCT images obtained for the furfurylated maple samples demonstrated that all ray cells and some vessel elements were filled with furan polymer while the fibers largely remained unchanged. Furfurylation significantly decreased the total porosity of both the maple and pine samples. Furthermore, this was observed in both earlywood (EW) and latewood (LW) regions in the pine samples. In contrast, the total porosity of pine samples was hardly affected by acetylation. These findings are in line with wetting results demonstrating that furfurylation reduces both swelling and capillary uptake in contrast to acetylation which reduces mostly swelling. Furfurylation significantly increased the cell wall thickness of both the maple and pine samples, especially at higher levels of furfurylation.

Keywords: acetylation, cell wall thickness, furfurylation, hardwood, microstructure, porosity, softwood, submicron X-ray computed tomography, tracheid, wettability

Introduction

Wood is modified to improve its decay resistance, dimensional stability, and weathering performance, and to reduce its water sorption (Hill 2006). Chemical modification changes the wood's chemical composition, wetting characteristics, biological durability, and mechanical properties. In short time, the modification changes the mechanisms related to cell wall swelling and the chemical properties of the cell wall matrix (Sander et al. 2003). Chemical modification leads to a permanent bulking of the cell wall in contrast to the reversible swelling due to water sorption. Mapping and visualization of these structural changes increase the understanding of the mechanism of chemical modification and facilitate the optimization of the modification parameters. Sander et al. (2003), Kwon et al. (2007) and Wålinder et al. (2009) studied microstructural changes induced by chemical modification of wood. For instance, acetylation was observed by electron microscopy (EM), and no evidence was found for cell wall damages or significant change in the microstructure

***Corresponding author: Maziar Sedighi Moghaddam,** SP Technical Research Institute of Sweden-Chemistry, Materials and Surfaces, Box 5607, SE-114 86 Stockholm, Sweden; and KTH Royal Institute of Technology, School of Architecture and the Built Environment, Department of Civil and Architectural Engineering, Building Materials, SE-100 44 Stockholm, Sweden,
e-mail: maziar.sedighi@sp.se
Jan Van den Bulcke and Joris Van Acker: UGCT – Laboratory of Wood Technology, Department of Forest and Water Management, Faculty of Bioscience Engineering, Ghent University, Coupure Links 653, 9000 Gent, Belgium
Magnus E.P. Wålinder: KTH Royal Institute of Technology, School of Architecture and the Built Environment, Department of Civil and Architectural Engineering, Building Materials, SE-100 44 Stockholm, Sweden
Per M. Claesson and Agne Swerin: SP Technical Research Institute of Sweden-Chemistry, Materials and Surfaces, Box 5607, SE-114 86 Stockholm, Sweden; and KTH Royal Institute of Technology, School of Chemical Science and Engineering, Department of Chemistry, Surface and Corrosion Science, SE-100 44 Stockholm, Sweden

(Sander et al. 2003). In another scanning electron microscopy (SEM) study (Wålinder et al. 2009), it was shown that some micro- structural changes may occur *in situ* polymerization during furfurylation, like polymer-filled lumen and microcracks in the cell walls. However, microstructural properties and remaining air-filled voids in acetylated and furfurylated wood samples are not yet quantified.

Microstructural features such as tracheid dimensions, cell wall thickness, total porosity, and porosity of certain cells and special tissues can all affect the macroscopic properties of wood (Trtik et al. 2007). The complex wetting phenomena including water uptake are affected by the 3D morphological characteristics of wood (Sedighi-Gilani et al. 2012). Bucur (2003) compiled several nondestructive imaging techniques for observation of wood morphology. Most of the routine techniques provide only 2D images and have a limited resolution. X-ray computed tomography (XCT), first developed for medical applications, is meanwhile an established technique to visualize 3D structures in wood at macro-, micro-, and nanometer scales also in wood science. A few examples may illustrate this: XCT was applied to study wood species (Trtik et al. 2007; Van den Bulcke et al. 2009; Svedström et al. 2012), wood coatings (Van den Bulcke et al. 2010; Bessières et al. 2013), structural changes during drying and modification (Leppänen et al. 2011; Van den Bulcke et al. 2011; Taylor et al. 2013; Biziks et al. 2016), archeological wood (Svedström et al. 2011), cork (Oliveira et al. 2016), fiberboards (Badel et al. 2008, Walter and Thoemen 2009), wood plastic composites (Defoirdt et al. 2010; Schwarzkopf and Muszynski 2015), plywood (Van den Bulcke et al. 2011), wood strand composites (Li et al. 2016), and wax-impregnation (Scholz et al. 2010a,b), just to mention a few. In general, the emerging synchrotron based TM with its high resolution has a great analytical power for wood research (Trtik et al. 2007; Hass et al. 2010; Zauner et al. 2012; Endo and Sugiyama 2013; Baensch et al. 2015).

In a previous study (Sedighi Moghaddam et al. 2016), the multicycle Wilhelmy plate method was utilized for determining wetting properties of chemically modified wood. The studies included water (as a swelling liquid) and the non-swelling octane, and it was demonstrated that acetylation reduces water uptake mainly by limiting the swelling. Conversely, the sorption data suggested that furfurylation diminishes both swelling and the void volume in the samples. Accordingly, there are significant microstructural differences between acetylated and furfurylated wood. One of the main motivations of the present study is to clarify these differences. The method of choice is XCT in order to visualize anatomical details and to quantify micro-structural properties, such as total porosity and the porosity of different cell types, cell wall thicknesses, and the size of tracheids after acetylation and furfurylation. The wetting properties of the modified samples should be rationalized by observation of microstructural changes induced by these modifications.

Materials and methods

One set of boards of Southern yellow pine (pine), *Pinus palustris*, with dimension of $40\times14\times2.5$ cm^3 (L×T×R) were acetylated in a pilot plant at SP in Borås, Sweden. The process was performed in a microwave-heated reaction vessel following procedures described in Rowell et al. (1985) leading to ca. 16 and 22% acetyl content of the samples ($pine_{acet16}$ and $pine_{acet22}$, respectively). Two unmodified matched samples from the same boards served as control samples ($pine_{ctrl16}$ and $pine_{ctrl22}$, respectively). The $pine_{ctrl16}$ has a growth ring width of 0.4–1.3 mm and a latewood (LW) portion of 61±9%, while the corresponding values of $pine_{ctrl22.2}$ were 1–1.8 mm and 37±9%, respectively. The furfurylation process was performed on another set of pine and maple samples in an autoclave by means of a pressure process, and cured and dried in a vacuum drying kiln at a pilot plant at Kebony AS, Porsgrunn, Norway, following procedures described in Lande et al. (2004). The following furfurylated samples were prepared: (1) $pine_{furf28}$ and $pine_{furf45}$ with weight percentage gain (WPG) of ca. 28 and 45%, respectively, and (2) furfurylated maple (*Acer platanoides*) ($maple_{furf32}$) with a WPG level of ca. 32%. The unmodified $pine_{ctrl}$ sample was the same as for $pine_{ctrl16}$. The $maple_{ctrl}$ was collected from the same board.

Needle shaped samples measuring approx. 5 mm (L), 1 mm (T) and 1 mm (R) and (or smaller) were cut with a razor blade from larger wood blocks. For each sample type (e.g. $pine_{acet22}$), two pure earlywood (EW) and LW samples were prepared. The samples were then dried at 104°C for 1 h in an oven in order to have the same conditions as for the wetting measurements (see below). The samples were then glued on a cylindrical pencil lead sample holder.

The central part of each needle shaped sample, measuring approx. $0.5\times0.5\times0.5$ mm^3 was scanned on an instrument Nanowood, which is a state-of-the-art X-ray CT scanner developed at UGCT at Ghent University, Belgium (Dierick et al. 2014). At least, two replicate samples were scanned for each sample type, and in total about 50 scans were performed. Samples were scanned at an average voltage of 90 kV with a rotation step size of 0.36°, a target current of 50 μA, and an exposure time of 2000 ms per image, resulting in an approx. scan time of 60 min per object. Reconstruction was performed by Octopus Reconstruction, a tomography reconstruction package for parallel, helical, and cone beam geometry (Vlassenbroeck et al. 2007) licensed by InsideMatters (www.insidematters.eu; Gent, Belgium), resulting in an approx. voxel pitch of 0.8 μm. A selection of samples was also investigated at the highest possible resolution of the scanner (0.4 μm). All scans were phase filtered with the Paganin algorithm. Reconstructed volumes were then processed with Morpho+ (Vlassenbroeck et al. 2007), a software package for volume analysis, currently known as Octopus Analysis, which is also licensed by InsideMatters. Volumes were median and

bilateral filtered for noise removal. Wood and air were distinguished by thresholding and the total porosity was calculated. The porosity of specific structural features (e.g. tracheids in softwood samples) was determined by automated labeling and subsequent manual selection of the anatomical features of interest. Cell wall (CW) thicknesses were calculated by MATLAB® (MathWorks, Natick, USA) (details in Van den Bulcke et al. 2009) and in supporting information. The porosity and cell wall thickness were measured in the 3D mode. All 3D reconstructed volumes were visualized by VGStudio MAX® (Volume Graphics, Heidelberg, Germany), while ImageJ® was used for visualization of 2D slices through the volume.

The wetting studies were performed on acetylated and furfurylated samples prepared in the same manner as those described for the microstructural studies. The multicycle Wilhelmy plate method that was employed according to Sedighi Moghaddam et al. (2016).

Results and discussion

2D microscopic structure

Phase and noise filtered 2D microstructural images of the specimens are illustrated in Figure 1 and Supplementary Figure S1. There are no visible microstructural differences at the 0.8 μm resolution level between acetylated and unmodified $pine_{EW}$ (Figure 1a,b). Tracheids are similar in size and shape and no significant changes are seen in cell wall thicknesses. Similar observations are noted for $pine_{LW}$ (Figure S1). These observations are consistent with SEM and TEM data reported for acetylated wood (Sander et al. 2003).

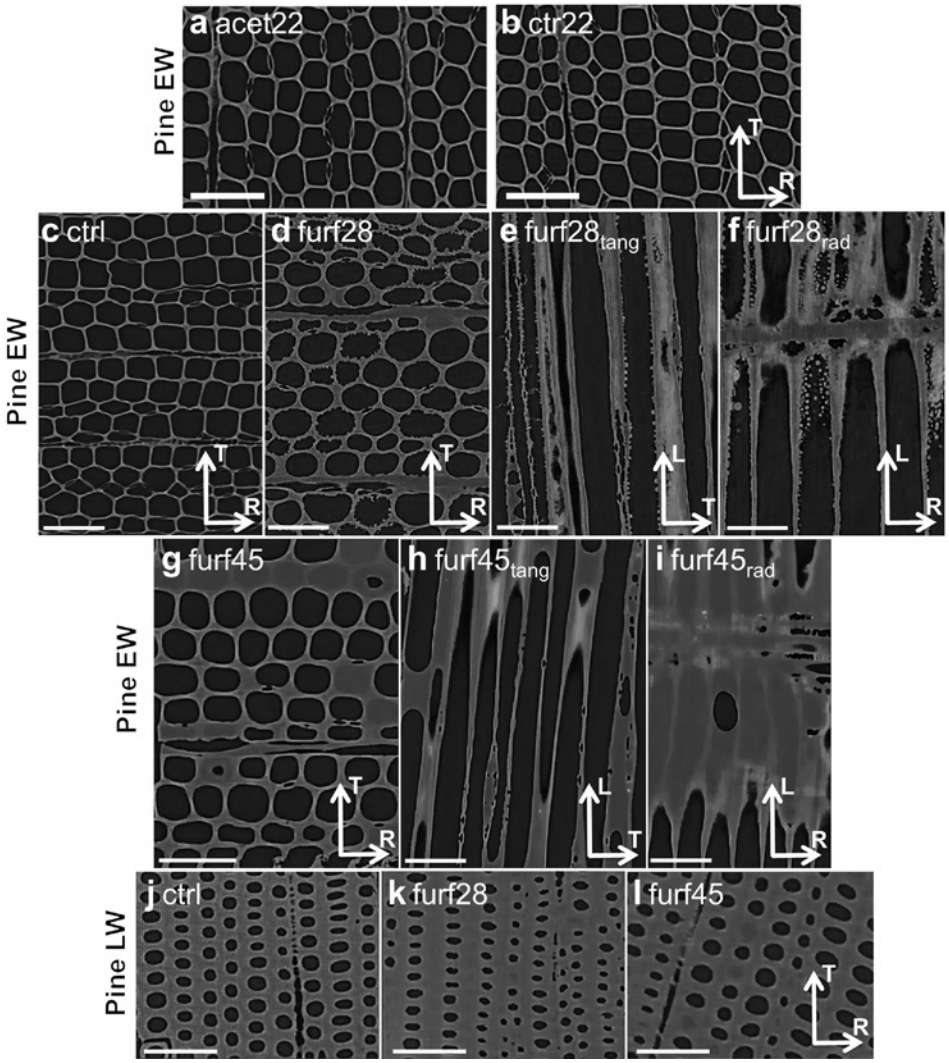

Figure 1: X-ray computed microtomography images of different samples.
Transverse sections of (a) acetylated pine EW ($pine_{acet22}$), (b) unmodified pine EW ($pine_{ctrl22}$), (c) unmodified pine, different sections of furfurylated pine EW ($pine_{furf28}$): (d) transverse, (e) tangential and (f) radial, different sections of furfurylated pine EW ($pine_{furf45}$): (g) transverse, (h) tangential and (i) radial, and transverse sections of LW samples: (j) unmodified pine, (k) $pine_{furf28}$ and (l) $pine_{furf45}$. The scale bar corresponds to 100 μm.

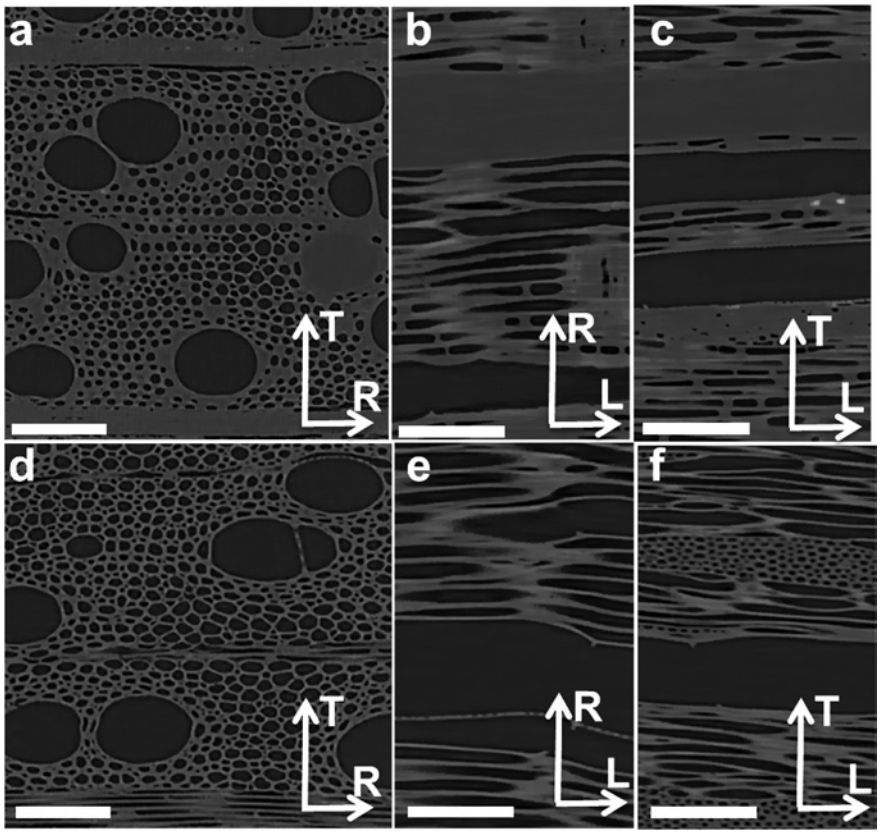

Figure 2: X-ray computed microtomography images of different sections of furfurylated maple ($maple_{furf32}$).
(a) Transverse, (b) radial and (c) tangential; and of unmodified maple ($maple_{ctrl}$): (d) transverse, (e) radial and (f) tangential cross-section.
The scale bars correspond to 100 μm.

Unlike the acetylated samples, significant changes in microstructural properties were detected for the furfurylated samples (Figure 1c–l for pine and Figure 2 for maple). As seen in Figure 1c, the majority of the tracheids in the transverse section of unmodified $pine_{EW}$ are rectangular, pentagonal or hexagonal in shape. However, at the lower level of furfurylation (WPG 28%) (Figure 1d), the apparent shape of these tracheids became more circular or elliptical. In addition, it is obvious that some tracheids were completely or partially filled with furan polymers. This is also illustrated in T and R cross-sectional images (Figure 1e,f). Furthermore, the cell walls of the furfurylated samples are clearly thicker than those of unmodified samples. Obviously, furfuryl alcohol leads to a swelling and, moreover, a formation of a polymer layer on the cell walls is clearly visible. At the higher level of furfurylation (WPG 45%), even more tracheids are filled with furan polymers (Figure 1g) and the cell walls seem to be slightly thicker compared to those of $pine_{furf28}$. This is consistent with the finding of Wålinder et al. (2009) concerning the higher filling ratio of lumens at higher WPG levels. Additionally, as illustrated in Figure 1h,i, the furfurylated tracheids are completely or partly filled. Furan polymer deposits can be found inside the LW tracheids as well, where some of the tracheids are completely filled (Figure 1k,l). The highest resolution of the scanner (0.4 μm) did not give additional information.

The XCT images of chemically modified maple sample are presented in Figure 2, where the effects of furfurylation are clearly seen. Extensive furan polymer deposits can be distinguished in the vessels, fibers, and rays. Ray cells were mostly filled, while only some of the vessels were filled and most of the fibers remained empty. Obviously, at higher WPG level, furfuryl alcohol more easily penetrates to the wood voids of rays and vessels, which will be discussed below.

3D microscopic structure

XCT allows 3D imaging of the wood structure without laborious sample preparation. The different impressions provided by 2D and 3D images are presented in Figure 3 that shows two transverse sections of the same furfurylated sample taken at different heights along the scanned volume. The same tracheid can thus appear

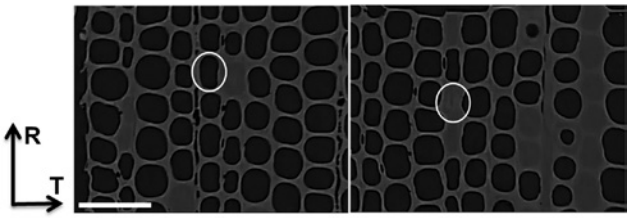

Figure 3: 2D X-ray computed microtomography images of transverse sections at two different heights, 530.4 µm apart, of a pine$_{furf45}$ EW sample.
The marked areas show the same tracheid. The scale bar corresponds to 100 µm.

either empty (left image) or filled (right image), if only 2D cross sections are imaged. The 3D working mode reveals more details and also allows for quantification of anatomical features. This is illustrated in Figures 4 and 5 showing furfurylated pine and maple samples. The deposition of furan polymers on the tracheid walls can be clearly seen (Figure 4a,b). Additionally, as seen in Figure 4c, the visualization of the 3D volume helps to understand the distribution and filling of tracheids with the furan polymer. The advantages of XCT compared to 2D SEM are obvious. After furfurylation, almost all rays were completely filled, while most of the fibers remained empty (Figure 5).

Morphological properties

Table 1 summarizes the data concerning total porosity, cell wall thickness (CWTh), maximum opening of tracheids, and wetting results. The CWTh was determined by excluding the cell corners. The maximum opening of a tracheid is defined as the diameter of the largest sphere that fits in the tracheid lumen, and it is thus a 3D parameter. For the acetylated samples (in both EW and LW areas), the total porosity is similar. Conversely, the results show that furfurylation significantly reduces the porosity of the samples in both EW and LW areas.

This can be related to the wetting results (Table 1, and details presented in Sedighi Moghaddam et al. 2016), where no changes in octane uptake were observed for acetylated samples. But changes occur in furfurylated wood. Figure 6 shows that the total porosity and octane uptake via capillary forces are related to each other for both acetylated and furfurylated pine and maple. The total porosity of each

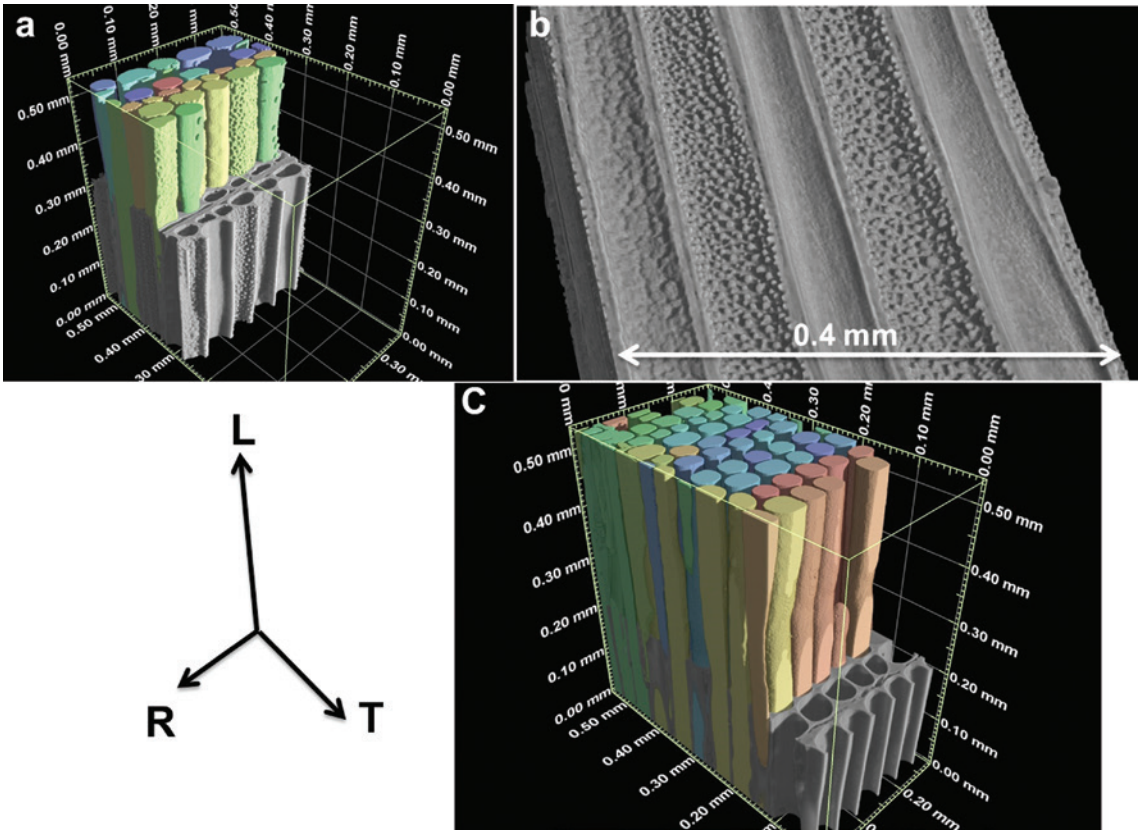

Figure 4: Volume rendering of pine$_{furf}$ EW with WPG of 28%.
(a) With randomly color labeled tracheid lumens except for the two first rows, (b) a zoomed view of the deposits on the tracheid cell wall; (c) randomly colour labeled tracheid lumens of furfurylated pine with WPG of 45%.

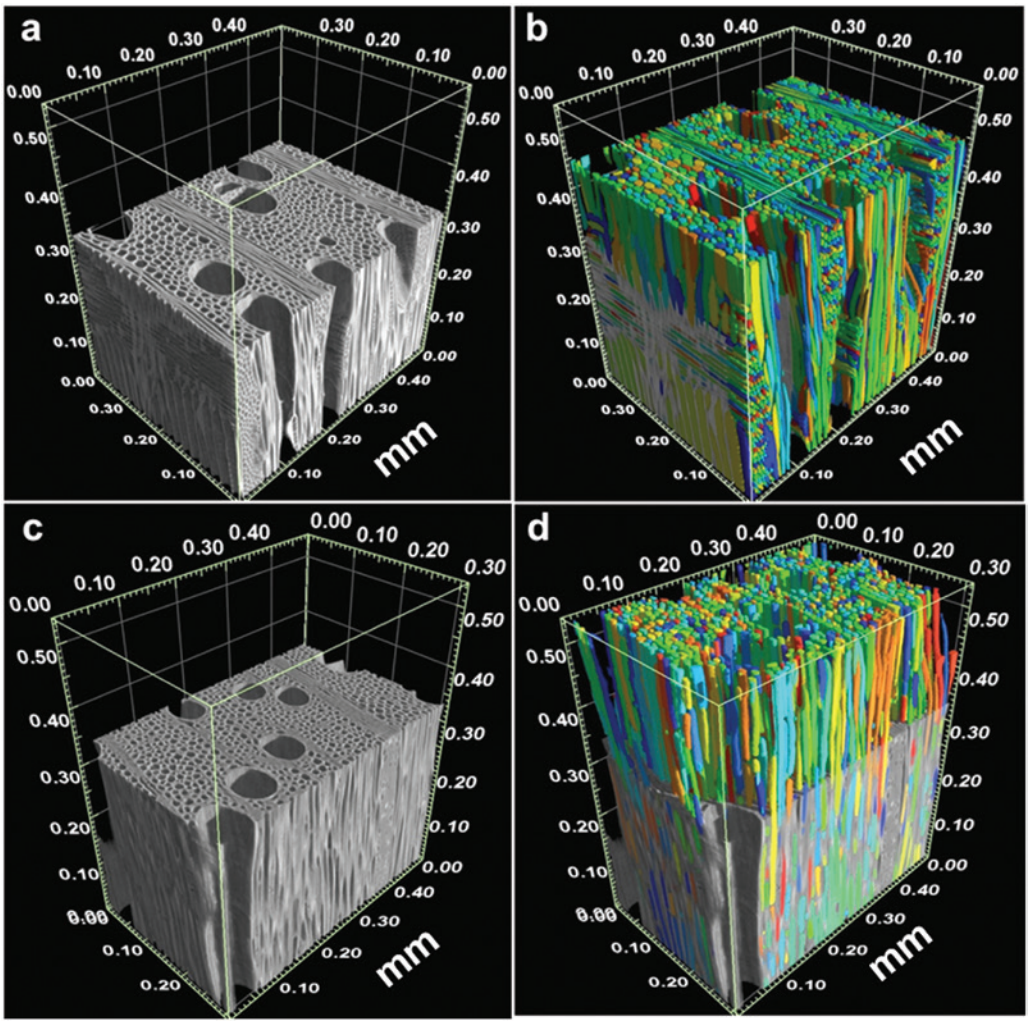

Figure 5: Volume rendering of (a) unmodified maple and (c) $maple_{furf}$ with WPG of 32%. Two other volume renderings show randomly color labeled tracheid lumens of the samples without vessels for (b) unmodified maple and (d) $maple_{furf}$.

specimen was calculated based on the EW/LW ratio of that specimen [measured with a digital caliper, Mitutoyo (Aurora, USA) with 0.01 mm accuracy] and the porosity of EW and LW volumes obtained by means of XCT. According to this relation, a wood sample with higher porosity has higher wicking and capillary uptake. For instance, an acetylated sample with approx. the same porosity as its control ($pine_{acet22}$), absorbed almost the same amount of octane in wetting measurements as the control, while a high-level furfurylated sample ($pine_{furf45}$) showed a significantly lower level of porosity and octane uptake compared to the unmodified sample ($pine_{ctrl16}$).

The porosity of different anatomical features can also be determined via the scanned volumes. An example is presented in Figure 7 that shows the total porosity and the porosity of the vessels, fibers, and rays for $maple_{furf32}$ and its corresponding control ($maple_{ctrl}$). The large variation in porosity (especially for vessels in the unmodified sample) is due to absence or presence of single large vessels in the scanned samples. The present study demonstrates that cell wall filling via furfurylation mostly occurs in rays and partly in some vessels, while the wood fibers were less affected. This findig is also reflected by the porosity reduction of the rays and vessels, whereas there are no changes with this regard in the fibers.

The CWTh, or more precisely the distance between two adjoining wood cells, was also evaluated (Table 1). The average CWTh (mean wall thickness for 50–100 tracheids) of the acetylated samples is similar to that of the unmodified samples, whereas the apparent CWTh in the furfurylated samples is significantly higher than that in the control samples of both EW and LW areas. Figure 8 shows the CWTh distribution for acetylated and furfurylated pine in EW and LW areas.

The CWTh shifts slightly to higher values for acetylated samples (Figure 8a,c) especially for LW regions

Table 1: Liquid uptake, total porosity, cell wall thickness and maximum opening of tracheid lumen of acetylated and furfurylated samples.

			Total porosity (%)		Cell wall thickn. (μm)		Max. open. trach. (μm)[a]
Sample	**Water uptake (%)**	**Octane uptake (%)**	**EW**	**LW**	**EW**	**LW**	**EW**
$Pine_{acet16}$	34.1±1.6	21.0±1.5	73.8±1.8	24.1±5.2	5.7±2.1	14.3±6.9	29.5±12.8
$Pine_{ctrl16}$	54.3±1.5	28.0±2.9	76.1±1.8	29.3±1.0	5.3±2.0	14.6±5.2	31.5±12.8
$Pine_{acet22}$	41.9±3.7	34.8±6.2	76.6±0.6	26.4±0.8	5.5±2.2	16.1±5.4	33.0±16.7
$Pine_{ctrl22}$	70.6±4.2	36.3±3.2	75.3±0.9	27.5±4.4	5.5±2.1	13.9±5.8	29.3±17.9
$Pine_{furf28}$	21.3±4.5	11.8±0.6	66.2±3.8	16.7±3.5	8.4±4.5	19.6±7.2	
$Pine_{furf45}$	12.7±1.5	8.5±0.7	61.1±2.7	18.0±1.0	9.2±5.0	19.2±8.3	33.3±19.8
$Maple_{furf32}$	13.9±2.4	9.6±1.4		38.9±1.3	nd	nd	nd
Maple	59.2±3.4	30.0±2.6		51.3±2.7	nd	nd	nd

[a]Maximal opening of tracheid lumen. Water and octane uptake are based on 20-cycle and 10-cycle Wilhelmy plate measurements, respectively (Sedighi Moghaddam et al. 2016).

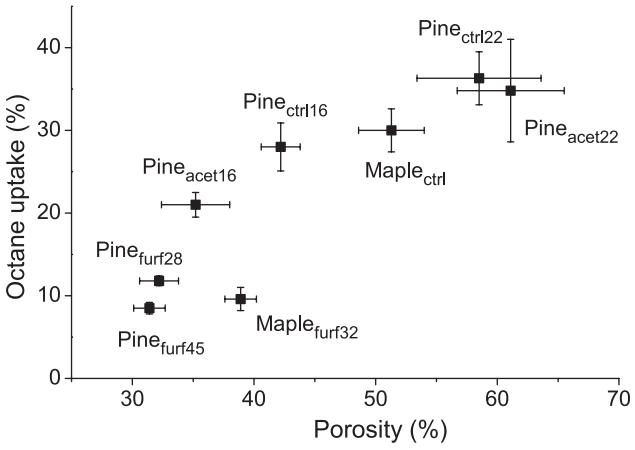

Figure 6: Octane uptake as a function of total porosity for different modified and unmodified wood samples.
The octane uptake and porosity results are based on four replicates. The porosity results are calculated based on porosity of EW and LW regions obtained from two XCT scans and EW/LW proportion of each replicate.

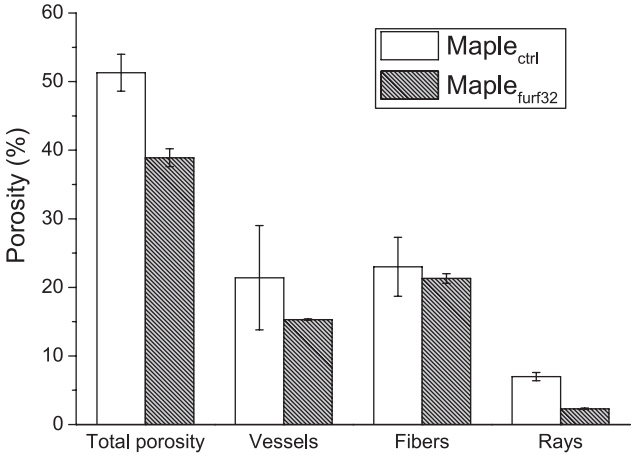

Figure 7: Total porosity and porosity of different microstructural components of $maple_{furf}$ and unmodified maple.

compared to the control samples, while this difference in apparent CWTh is significantly larger for furfurylated samples especially in LW areas (Figure 8d). Additionally, the wood cell walls are thicker at the high-level furfurylation ($pine_{furf45}$) than in a low-level one ($pine_{furf28}$) in both EW and LW areas. It should be noted that a thick layer of furan polymer was deposited on the cell wall, which means that the lumen size decreases and the apparent CWTh increases, i.e. the observed increase in CWTh is a result of swelling and layer deposition.

There is no difference concerning the mean value of the maximum opening of tracheid lumens for modified and unmodified samples (Table 1). On the other hand, the maximum opening of tracheid lumens is not sufficient to characterize the effect of the chemical modification because the tracheids can be partly filled (Figure 4) and this might not affect the maximum opening of the lumens. Another geometrical descriptor, the equivalent diameter (ED) of the tracheid, was introduced for characterizing the micromorphological changes. ED is defined as the diameter of a sphere with a volume equivalent related to the volume of the tracheid. Figure 9 illustrates the maximum opening of the tracheid lumens as a function of ED for the unmodified and modified samples. When the size of the tracheids is homogeneous in a sample, their ED increases linearly with the maximum opening, which can be noted for unmodified pine (Figure 9a). However, in case of modified samples (Figure 9b–d), the results are more scattered due to the morphological changes inside the tracheids. For instance, two tracheids with the same maximum opening might have different equivalent diameters as a result of the furan polymer deposits inside the wood structure (Figure 9c,d). This is most probably caused by a permanent bulking in case of chemically modified wood. These changes are much more pronounced for furfurylated samples than for acetylated ones (Figure 9b with 9c,d).

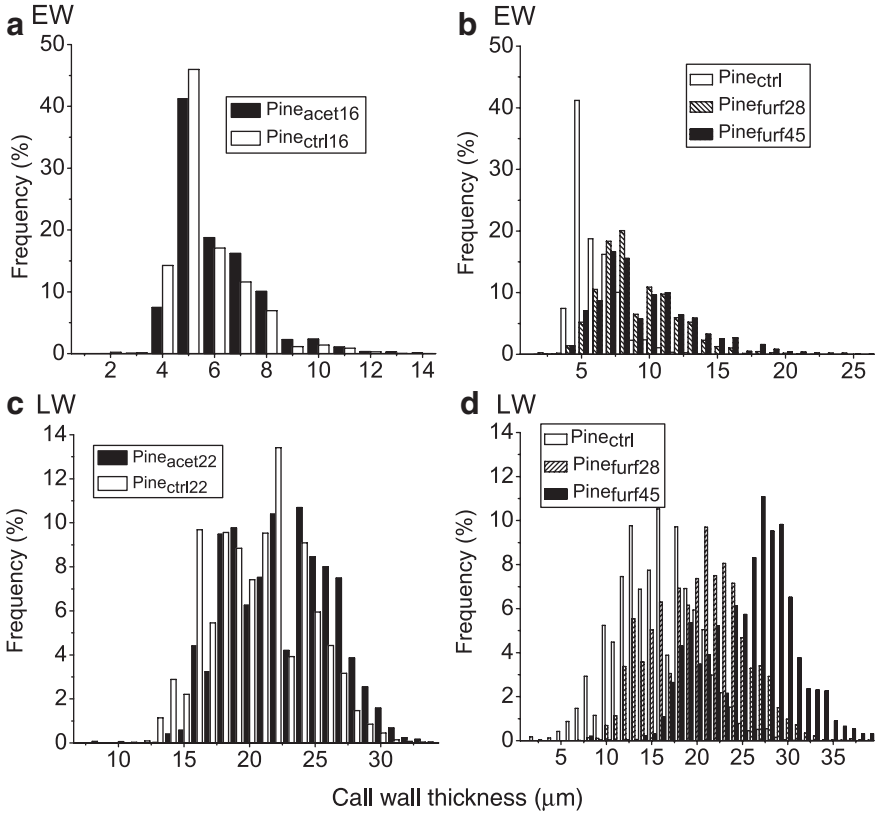

Figure 8: Distribution of the cell wall thickness (CWTh), for (a) acetylated pine EW, (b) furfurylated pine EW, (c) acetylated pine LW and (d) furfurylated pine LW.

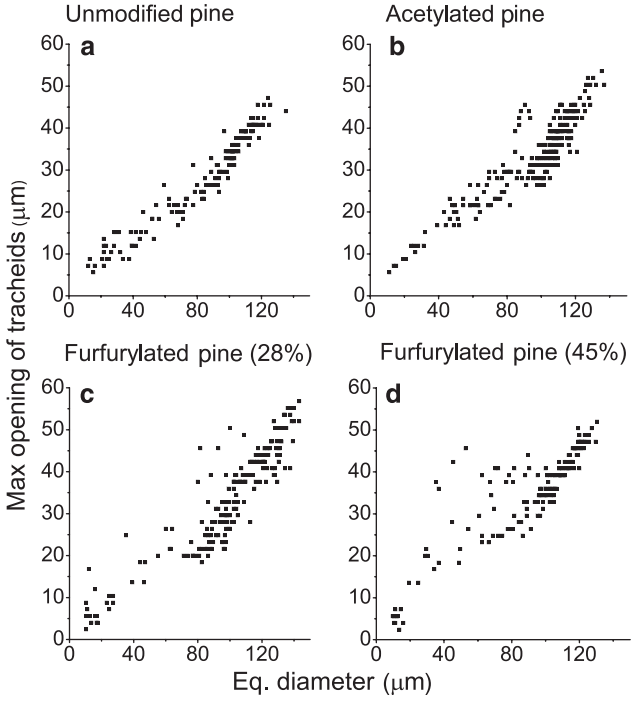

Figure 9: Maximum opening as a function of equivalent diameter of tracheid lumens for pine EW of: (a) unmodified, (b) acetylated, (c) furfurylated with a WPG of 28% and (d) furfurylated with a WPG of 28%.

Additionally, the sample with the higher furan polymer content (pine$_{furf45}$, Figure 9d) is also more heterogeneous in terms of tracheid size than the sample with lower level of WPG (pine$_{furf28}$, Figure 9c).

Conclusions

The microstructure of acetylated and furfurylated pine and maple samples was investigated by XCT. This facilitated quantitative measurements of anatomical changes in wood caused by the chemical modification. In particular, the total porosity and the porosity of different anatomical features were determined, such as the cell wall thickness and the tracheid lumen size. Significant micro- structural changes were observed for pine$_{furf}$ and maple$_{furfur}$. This was mainly visible on change in tracheid shape and filling of tracheids by furan polymer in the sapwood samples and filling of all ray cells and some vessels in case of maple$_{furf}$. Conversely, acetylated samples did not reveal significant changes even at the high resolution of 0.8 μm. By porosity measurements, it was also possible to elucidate which anatomical features that were most strongly affected by the chemical modification. The microstructural

characteristics (mainly the capillarity) strongly affect wetting properties. The porosity of the pine$_{furf}$ decreased due to the chemical modification, which was not the case for pine$_{acet}$. The wetting results revealed that acetylation predominantly reduces swelling, while furfurylation reduces both swelling and capillary uptake. The average cell wall thickness (CWTh) of acetylated samples was similar to that of unmodified ones, however, the distribution profile of the CWTh shifts slightly to higher values. For furfurylated samples, the apparent CWTh was significantly higher in both EW and LW areas compared to the unmodified control samples. This is due to the combined effect of swelling and deposition of a thick layer of furan polymer on the cell wall. Furfurylation also diminishes the tracheid lumen size.

Acknowledgments: Financial support by the Transnational Access to Research Infrastructures activity in the 7th Framework Programme of the EC under the Trees4Future project (no. 284181) for conducting the research is gratefully acknowledged. The authors also thank the Nils and Dorthi Troëdsson Foundation for Scientific Research for financial support within the sustainable wood modification PhD project for M.S.M. and the adjunct professorship for A.S. at KTH. Swedish Research Council FORMAS within the EnWoBio project (2014-172) provided additional funding.

References

Badel, E., Delisee, C., Lux, J. (2008) 3D structural characterisation, deformation measurements and assessment of low-density wood fibreboard under compression: The use of X-ray microtomography. Compos. Sci. Technol. 68:1654–1663.

Baensch, F., Zauner, M., Sanabria, S.J., Sause, M.G.R., Pinzer, B.R., Brunner, A.J., Stampanoni, M., Niemz, P. (2015) Damage evolution in wood: synchrotron radiation micro-computed tomography (SRμCT) as a complementary tool for interpreting acoustic emission (AE) behavior. Holzforschung 69:1015–1025.

Bessières, J., Maurin, V., George, B., Molina, S., Masson, E., Merlin, A. (2013) Wood-coating layer studies by X-ray imaging. Wood Sci. Technol. 47:853–867.

Biziks, V., Van den Bulcke, J., Grinins, J., Militz, H., Andersons, B., Andersone, I., Dhaene, J., Van Acker, J. (2016) Assessment of wood microstructural changes after one-stage thermo-hydro treatment (THT) by micro X-ray computed tomography. Holzforschung 70:167–177.

Bucur, V. Nondestructive Characterization and Imaging of Wood, Springer, Heidelberg, 2003.

Defoirdt, N., Gardin, S. Van den Bulcke, J., Van Acker, J. (2010) Moisture dynamics of WPC and the impact on fungal testing. Int. Biodeter. Biodegr. 64:65–72.

Dierick M., Loo, D.V., Masschaele, B., Van den Bulcke, J., Van Acker, J., Cnudde, V., Van Hoorebeke, L. (2014) Recent micro-CT scanner developments at UGCT. Nucl. Instrum. Meth. B. 324:35–40.

Endo, R., Sugiyama, J. (2013) Evaluation of cell wall reinforcement in feather keratin-treated waterlogged wood as imaged by synchrotron X-ray microtomography (μXRT) and TEM. Holzforschung 67:795–803.

Hass, P., Wittel, F.K., McDonald, S.A., Marone, F., Stampanoni, M., Herrmann, H.J., Niemz, P. (2010) Pore space analysis of beech wood: The vessel network. Holzforschung 64:639–644.

Hill, C.A.S. (2006) Modifying the properties of wood. In: Wood Modification. John Wiley & Sons, Ltd., West Sussex. pp. 19–44.

Kwon, J.H., Hill, C.A.S. Ormondroyd, G.A., Karim., S. (2007) Changes in the cell wall volume of a number of wood species due to reaction with acetic anhydride. Holzforschung 61:138–142.

Lande, S., Westin, M., Schneider, M. (2004) Properties of furfurylated wood. Scand. J. For. Res. 19(sup5):22–30.

Leppänen, K., Bjurhager, I., Peura, M., Kallonen, A., Suuronen, J.-P., Penttilä, P., Love, J., Fagerstedt, K., Serimaa, R. (2011) X-ray scattering and microtomography study on the structural changes of never-dried silver birch, European aspen and hybrid aspen during drying. Holzforschung 65:865–873.

Li, P., Tao, Y., Wu, Q. (2016) A three-dimensional void reconstruction method for analyzing fractal dimensions of void volume in wood-strand composites. Holzforschung 70:377–382.

Oliveira, V., Van den Bulcke, J., Van Acker, J., de Schryver, T., Pereira, H. (2016) Cork structural discontinuities studied with X-ray microtomography. Holzforschung 70: 87–94.

Rowell, R.M., Simonson, R., Tillman, A.-M. (1985) A process for improving dimensional stability and biological resistance of lignocellulosic materials. European Patent 0213252.

Sander, C., E. P. J. Beckers, Militz, H., van Veenendaal, W. (2003) Analysis of acetylated wood by electron microscopy. Wood Sci. Technol. 37:39–46.

Scholz, G., Van den Bulcke, J., Boone, M., Zauer, M., Bäucker, E., Van Acker, J., Militz, H., (2010a) Investigation on wax-impregnated wood. Part 1: Microscopic observations and 2D X-ray imaging of distinct wax types. Holzforschung 64:581–585.

Scholz, G., Van den Bulcke, J., Van Loo, D., Pfriem, A., Van Acker, J., Militz, H. (2010b). Investigation on wax-impregnated wood. Part 2: study of void spaces filled with air by He pycnometry, Hg intrusion porosimetry, and 3D X-ray imaging. Holzforschung 64:587–593.

Sedighi-Gilani, M., Griffa, M., Mannes, D., Lehmann, E., Carmeliet, J., Derome, D. (2012) Visualization and quantification of liquid water transport in softwood by means of neutron radiography. Int. J. Heat Mass Tran. 55:6211–6221.

Sedighi Moghaddam, M., Wålinder, M., Claesson, P., Swerin, A. (2016) Wettability and swelling of acetylated and furfurylated wood analyzed by multicycle Wilhelmy plate method. Holzforschung 70:69–77.

Svedström, K., Bjurhager, I., Kallonen, A., Peura, M., Serimaa, R. (2011) Structure of oak wood from the Swedish warship Vasa revealed by X-ray scattering and microtomography. Holzforschung 66:355–363.

Svedström, K., Lucenius, J., Van den Bulcke, J., Van Loo, D., Immerzeel, P., Suuronen, J.P., Brabant, L., Van Acker, J., Saranpää, P., Fagerstedt, K., Mellerowicz, E., Serimaa, R. (2012)

Hierarchical structure of juvenile hybrid aspen xylem revealed using X-ray scattering and microtomography. Trees 26: 1793–1804.
Schwarzkopf, M., Muszynski, L. (2015) Strain distribution and load transfer in the polymer-wood particle bond in wood plastic composites. Holzforschung 69:53–60.
Taylor, A., Plank, B., Standfest, G., Petutschnigg, A. (2013) Beech wood shrinkage observed at the micro-scale by a time series of X-ray computed tomographs (μXCT). Holzforschung 67:201–205.
Trtik, P., Dual, J., Keunecke, D., Mannes, D., Niemz, P, Stähli, P., Kaestner, A., Groso, A., Stampanoni, M. (2007) 3D imaging of microstructure of spruce wood. J. Struct. Biol. 159:46–55.
Van den Bulcke, J., Boone, M., Van Acker, J., Stevens, M., Van Hoorebeke, L. (2009) X-ray tomography as a tool for detailed anatomical analysis. Ann. For. Sci. 66:508–508.
Van den Bulcke, J., Boone, M., Van Acker, J., Van Hoorebeke, L. (2010) High-resolution X-ray imaging and analysis of coatings on and in wood. J. Coating Technol. Res. 7:271–277.
Van den Bulcke, J., De Windt, I., Defoirdt, N., De Smet, J., Van Acker, J. (2011) Moisture dynamics and fungal susceptibility of plywood. Int. Biodeter. Biodegr. 65:708–716.
Vlassenbroeck, J., Dierick, M., Masschaele, B., Cnudde, V., Van Hoorebeke, L., Jacons, P. (2007) Software tools for quantification of X-ray microtomography at the UGCT. Nucl. Instrum. Meth. A. 580:442–445.
Walter, T., Thoemen, H. (2009) Synchrotron X-ray microtomography and 3D image analysis of medium density fiberboard (MDF). Holzforschung 63:581–587.
Wålinder, M., Omidvar, A., Seltman, J., Segerholm, K. (2009) Micromorphological studies of modified wood using a surface preparation technique based on ultraviolet laser ablation. Wood Mater. Sci. Eng. 4:46–51.
Zauner, M., Keunecke, D., Mokso, R., Stampanoni, M., Niemz, P. (2012) Synchrotron-based tomographic microscopy (SbTM) of wood: development of a testing device and observation of plastic deformation of uniaxially compressed Norway spruce samples. Holzforschung 66:973–979.

Supplemental Material: The online version of this article (DOI: 10.1515/hf-2015-0227) offers supplementary material, available to authorized users.